Journal of The Electrochemical Society, **154** (3) J109-J115 (2007)
0013-4651/2007/154(3)/J109/7/$20.00 © The Electrochemical Society

Properties of Carbon Nanotubes Via a Thin Ti Capping Layer on the Pretreated Catalyst

Rui-Ling Lai,[z] Jiun-Kai Shiu, Yao-Ren Chang, Kao-Chao Lin, Pei-Chi Chang, Chuan-Pin Juan, Han-Chung Tai, and Huang-Chung Cheng

Department of Electronics Engineering and Institute of Electronics, National Chiao Tung University, Hsinchu 300, Taiwan

Screening effect and reliability are two of the most important issues in carbon nanotube-based field-emission devices. A thin Ti capping layer has been deposited on the hydrogen-pretreated catalytic iron nanoparticles to control the density of subsequently grown carbon nanotubes. In this way, the screening effect can be remarkably reduced due to the density of carbon nanotubes down to 10^7 from 10^9 cm^{-2} as compared to the control specimens. Thus, the turn-on field can be improved to be 2.1 from 3.8 V/μm at the emission current density of 10 $\mu A/cm^2$. Furthermore, the electrical breakdown field can be increased to more than 7 V/μm and the lifetime of carbon nanotubes at high electric field (10 V/μm) can be greatly prolonged from a few seconds to more than 1 h. This can be attributed to better adhesion and lower contact resistance between the carbon nanotubes and the substrate.
 [DOI: 10.1149/1.2426872]

Manuscript submitted July 26, 2006; revised manuscript received October 11, 2006. Available electronically January 30, 2007.

Carbon nanotubes have attracted a lot of attention since their first observation by Iijima in 1991.[1] Several methods have been developed to synthesize carbon nanotubes, such as arc discharge,[2] plasma-enhanced chemical vapor deposition (PE-CVD),[3] electron cyclotron resonance-CVD (ECR-CVD),[4] MP-CVD,[5] and thermal-CVD.[6,7] Because of many unique physical and chemical properties of carbon nanotube, it has been considered as a very potential material in many applications, such as, electronic devices,[8] hydrogen storage,[9] scanning probes,[10] and flat-panel displays.[11] Among them, flat panel displays fabricated using carbon nanotubes as electron emitters has been recognized one of the most promising technologies for the future.[12,13] The theory of field emission, Fowler-Nordheim tunneling, was published in 1928[14,15] and many materials and device structures have been developed to realize efficient emitters[16] since then. Due to the high aspect ratio, low work-function, great conductivity, high mechanical strength, high chemical inert, high thermal conductivity, and the ability of selective growth, carbon nanotubes are a wonderful electron emitting sources in field emission displays. However, some critical issues such as screening effect, reliability, uniformity, high driving voltage, and issues of packaging, have been often observed when carbon nanotubes were used as the electron emitters in field-emission displays.

According to the simulation of an electric field,[17] the best density of carbon nanotubes with 1 μm in length to suppress the screening effect and obtain an optimized emission current density is about 3×10^7 cm^{-2}. Unfortunately, the density of carbon nanotubes synthesized via CVD systems is much higher than 10^7 cm^{-2}. Several methods, such as SiOx capping,[18] plasma post-treatment,[19] E-beam lithography,[20] catalytic particle size control,[21] etc., have been reported to reduce the density of carbon nanotubes grown by CVD systems to suppress the screening effects. Although some of these methods can efficiently control the density of carbon nanotubes, there are still some problems, such as the destruction of crystallinity and the high cost of complex processes.

For reliability, it can generally be divided into two parts—electrical breakdown, an abrupt drop of emission current when the electric field between anode and cathode is increased,[22] and emission current degradation, a slow degradation of emission current when a constant electric field is applied between anode and cathode for a long period.[23,24] Okai et al.,[22] have shown that the electrical breakdown may result from a mechanical destruction of carbon nanotubes caused by a strong static electric force. From Bonard and Klinke's work,[24] the high contact resistance caused by the bad interface between the carbon nanotubes and the substrate with a high emission current density passing through will result in Joule heating and lead to local evaporation of carbon nanotubes. To suppress these two phenomena, we must increase the adhesion and reduce the contact resistance between the carbon nanotubes and the substrate. Different interfacial layer,[25,26] thermal treatment, spin-on-glass (SOG) coating,[27] and binder coating[28] have been used to improve the adhesion between carbon nanotubes and the substrate, but many of them cannot reduce the contact resistance between carbon nanotubes and the substrates at the same time.

Therefore, a thin Ti capping layer deposited on hydrogen-pretreated iron nanoparticles is proposed to suppress the screening effect and even to improve the reliability. With different thicknesses of the Ti capping layer, the density of carbon nanotubes can be controlled in a simple way without serious destructive effects in crytallinity and a high cost for excess processes, and the emission current density was remarkably increased due to the suppressing of the screening effect. Moreover, the electrical breakdown field and lifetime can also be improved, resulting from better adhesion and lower contact resistance between carbon nanotubes and the substrate.

Experimental

In our experiment, an n-type silicon wafer (100) with low resistance was used as the substrate. A 50×50 array of square holes with the dimension of 10×10 μm and 10 μm interspace were patterned by a lithography system (Fig. 1a). A 50 nm thick Ti layer was deposited by an E-beam evaporation system as a buffer layer and a 5 nm thick Fe layer was deposited subsequently as catalytic metal in the same system (Fig. 1b). Photoresistance was removed by a lift-off process in an ultrasonic vibration tank with acetone and only Fe/Ti (5/50 nm) in the holes was left after the lift-off process (Fig. 1c). After that, the sample was pretreated in the thermal-CVD furnace in atmospheric pressure at 700°C with H_2 (500 sccm) for 5 min to form catalytic iron nanoparticles (Fig. 1d). After the formation of catalytic nanopartibles, a thin Ti capping layer with different thicknesses (10, 20, 40, 100, and 200 Å) was deposited in a sputtering system (Fig. 1e). Then, the samples were loaded into the thermal-CVD furnace to grow carbon nanotubes in atmospheric pressure at 700°C with C_2H_4 (5 sccm) for 10 min (Fig. 1f).

After the growth of carbon nanotubes, the emission current from cathode electrode (silicon wafer) to anode electrode [(ITO) glass] was measured by Keithley 237 and Keithley 238 in a vacuum chamber at about 5×10^{-6} Torr with spacer about 100 μm from the cathode to the anode. Scanning electron microscope (SEM) images were taken by using Hitachi S-4700I to analyze the morphologies of samples. Furthermore, transmission electron microscopy (TEM) images and the Raman spectra analysis were conducted to analyze the

[z] E-mail: lary.ee91g@nctu.edu.tw

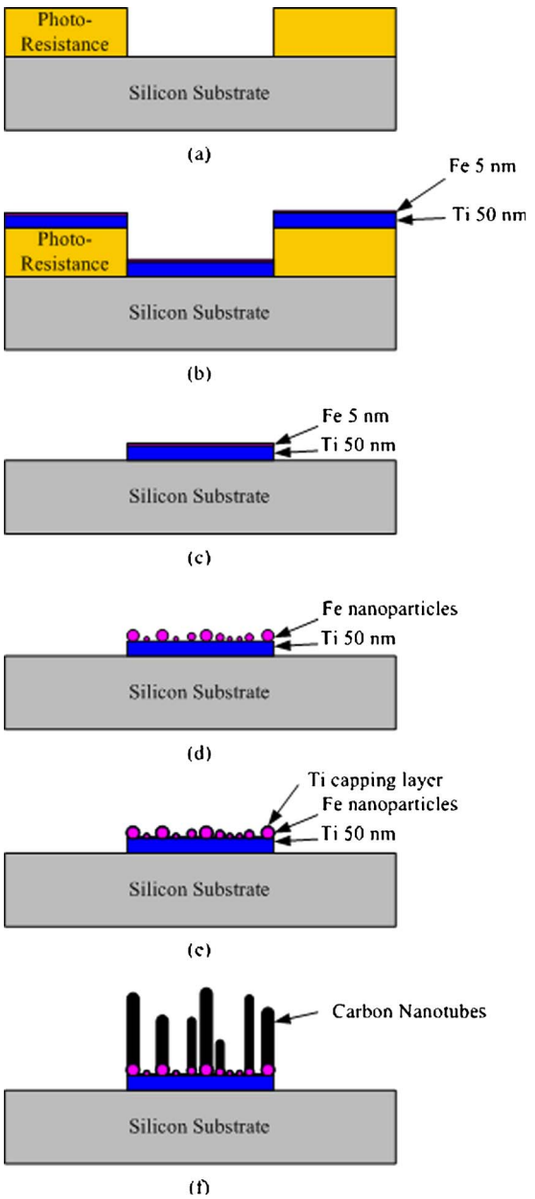

Figure 1. (Color online) Flowchart of the experiment: (a) An array of 10 μm in square holes was formed by a lithography system, (b) Ti (50 nm) and Fe (5 nm) were deposited by E-beam evaporation system, (c) photoresistance was removed via a lift-off process in an ultrasonic vibration tank with acetone, (d) samples were hydrogen-pretreated in the thermal-CVD, (e) a thin Ti capping layer with different thicknesses was deposited on the catalytic nanoparticles via a sputtering system, and (f) carbon nanotubes were synthesized in the thermal-CVD.

crystallinity of carbon nanotubes and energy dispersive spectrometer (EDS) was used to get the content of the nanoparticles in carbon nanotubes.

Results and Discussion

The SEM images of hydrogen-pretreated iron catalytic nanoparticles with different thicknesses of the thin Ti capping layer are shown in Fig. 2. Figures 2a-d show that part of catalytic nanoparticles remained and that the other particles become unobvious when the thickness of thin Ti capping layer is increased from 0 to 40 Å. This may be due to the fact that the catalytic nanoparticles with very small size are buried under the increased Ti capping layer. As the thickness of the Ti capping layer increased to 100 or 200 Å, the samples in the SEM images have only rough surfaces but obvious nanoparticles (as shown in Fig. 2e and f). After the deposition of the thin Ti capping layer, the samples are loaded into the thermal-CVD to grow carbon nanotubes. The SEM images in Fig. 3 show the morphologies of subsequently-grown carbon nanotubes. From the SEM images in Fig. 3a-e, it can easily be observed that the density of carbon nanotubes decreases with the increase in the thickness of the thin Ti capping layer. When the thickness of the Ti capping layer increased to 200 Å, there is no visible carbon nanotube on the substrate as shown in Fig. 3f. This shows that the thin Ti capping layer on pretreated catalytic nanoparticles can restrain the growth of carbon nanotubes and the density of carbon nanotubes can be controlled by changing the thickness of the thin Ti capping layer. As a speculation, the thin Ti capping layer can block the carbon radicals from diffusing into the catalytic nanoparticles so that the growth of carbon nanotubes is suppressed and the density is also altered. After the growth of carbon nanotubes, TEM images of carbon nanotube for samples with 20 Å Ti capping layer were taken and a nanoparticle was enclosed in the carbon nanotube as shown in Fig. 4a, with higher resolution in Fig. 4b, a well multiwall structure is observed. The normalized Raman spectra of CNTs for samples with 0, 10, and 20 Å Ti capping layers is shown in Fig. 5 (the signals of samples with thicker Ti capping layers were too weak to be detected). The results of Raman spectra were similar, which may indicate that there was no serious change in the crytallinity between the CNTs with and without the thin Ti capping layer. Moreover, an EDS analysis in Fig. 6 shows the component of the particle in the carbon nanotube. In the EDS analysis, three peaks of iron and one peak of carbon are observed. The peaks of copper are from the copper grid, which is used to hold the carbon nanotubes in TEM system. From the TEM images and the EDS analysis, Ti seems not to be involved into the catalytic nanoparticle and there is no obvious destructive affection on the crystallinity of the multiwall structure.

The curves of emission current density versus electric field (J-E curve) are shown in Fig. 7, which shows that the emission current density is relative to the thickness of the thin Ti capping layer. The Fowler-Nordheim plot (F-N plot) displayed in Fig. 7b can show that the measured emission current is a Fowler-Nordheim tunneling phenomenon. The field emission occurred in the samples with thin Ti capping layer above 40 Å. This implies that there were still CNTs in the samples with Ti capping layer above 40 Å, although the CNTs can hardly be observed in SEM images. However, the emission currents were almost negligible compared with samples to thin Ti capping layers below 40 Å. As shown in Fig. 7a, the emission current density is improved from 10 to 100 mA/cm^2 at 6 V/μm by increasing the thickness of the Ti capping layer from 0 to 20 Å. If the thickness of the Ti capping layer is over 20 Å, the emission current density reduces with the increase of thickness. The emission current is almost zero when the thickness of the Ti capping layer is 200 Å. This is consistent with the results of SEM images in Fig. 3f. The turn-on field ($E_{\text{turn-on}}$) and the threshold field (E_{th}) of these six samples are listed in Table I. To estimate the density of carbon nanotubes, SEM images from top view are taken and the approximate densities of six different samples are counted and shown in Table II. According to the results of electric field simulation of carbon nanotubes,[17] the most appropriate density for carbon nanotubes to obtain an optimized emission current density in the diode structure is about 3×10^7 cm^{-2}. Concluding from the J-E curves in Fig. 7a and the densities of carbon nanotubes in Table II, the density of carbon nanotubes which have the highest emission current density is about 2×10^7 cm^{-2} and the thickness of the thin Ti capping layer is 20 Å in this experiment. The experimental results here are very similar to the simulation in Ref. 17. From Table II, the turn-on field and the threshold field do not always decrease with the increase in the thickness of the thin Ti capping layer. The rise of the turn-on field when the thickness of the thin Ti capping layer is 100 Å may result from the decrease in the length of carbon nanotubes. From the SEM images in Fig. 3e, the length of carbon nanotubes is greatly

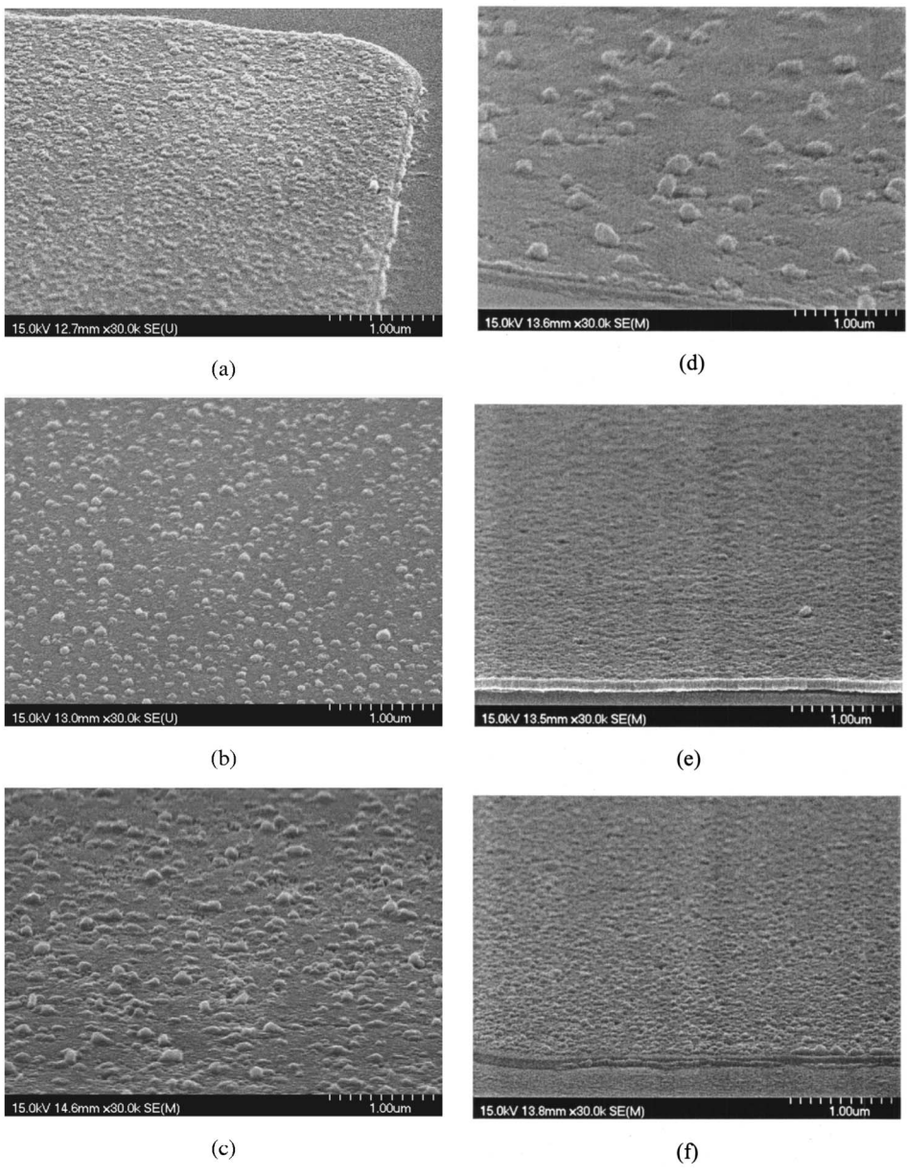

Figure 2. SEM images of hydrogen-pretreated catalytic nanoparticles with different thicknesses of the thin Ti capping layer: (a) 0, (b) 10, (c) 20, (d) 40, (e) 100, and (f) 200 Å.

reduced and result in the reduction of aspect ratio, which can lead to the decrease of the local field enhancement factor. Additionally, the rise of the threshold field when the thickness of thin Ti capping layer is 40 Å may be due to the reduction of emitting sites. Referring to the simulation results, the emission current density is also relative to the number of emission sites. By controlling the thickness of the thin Ti capping layer, it is possible to modify the electric characteristics of carbon nanotubes simply to gain an optimized emission current density.

Reliability is the other critical issue for carbon-nanotube-based field-emission devices discussed here. In this experiment, two methods were used to verify the reliability of carbon nanotubes—application of an electric field between the anode and the cathode and application of a strong electric field between the anode and the cathode for 1 h. A 50 Å thick Ti capping layer was deposited on the pretreated catalytic nanoparticles to compare with the conventional one. The curves of J-E for the first case, shown in Fig. 8, display an electrical breakdown which occurred on the carbon nanotubes without the thin Ti capping layer when the electric field reaches 6 V/μm. The morphologies of carbon nanotubes after electrical breakdown were taken by SEM and the sample with a thin Ti capping layer had no obvious change in SEM images. However, for the sample without a thin Ti capping layer, part of carbon nanotubes was pulled from the substrate (as shown in Fig. 9). This shows a mechanical destruction during the electrical breakdown. Referring to the paper of Okai et al., a similar result implies that a strong static electric force may be the main reason of the electrical breakdown in field-emission measurements. As the electric field between the anode and the cathode is increased, the dipole resulting from the concentrating of electrons in the tips of carbon nanotubes will enhance the static electric force and pull the carbon nanotubes off from the substrate therefore leads to an abrupt drop of emission current. This phenomenon is attributed to a poor adhesion between carbon nanotubes and the substrate. With a thin Ti capping layer on hydrogen-pretreated catalytic nanoparticles, there is no obvious electrical breakdown as the electric field is increased. This may be due to the better adhesion between catalytic nanoparticles and carbon nanotubes which result from the thin Ti capping layer. For the second part, a high electric field (10 V/μm) was applied between the anode and the cathode for 1 h and the emission current density vs time is shown in Fig. 10. As shown in Fig. 10a, the emission current density

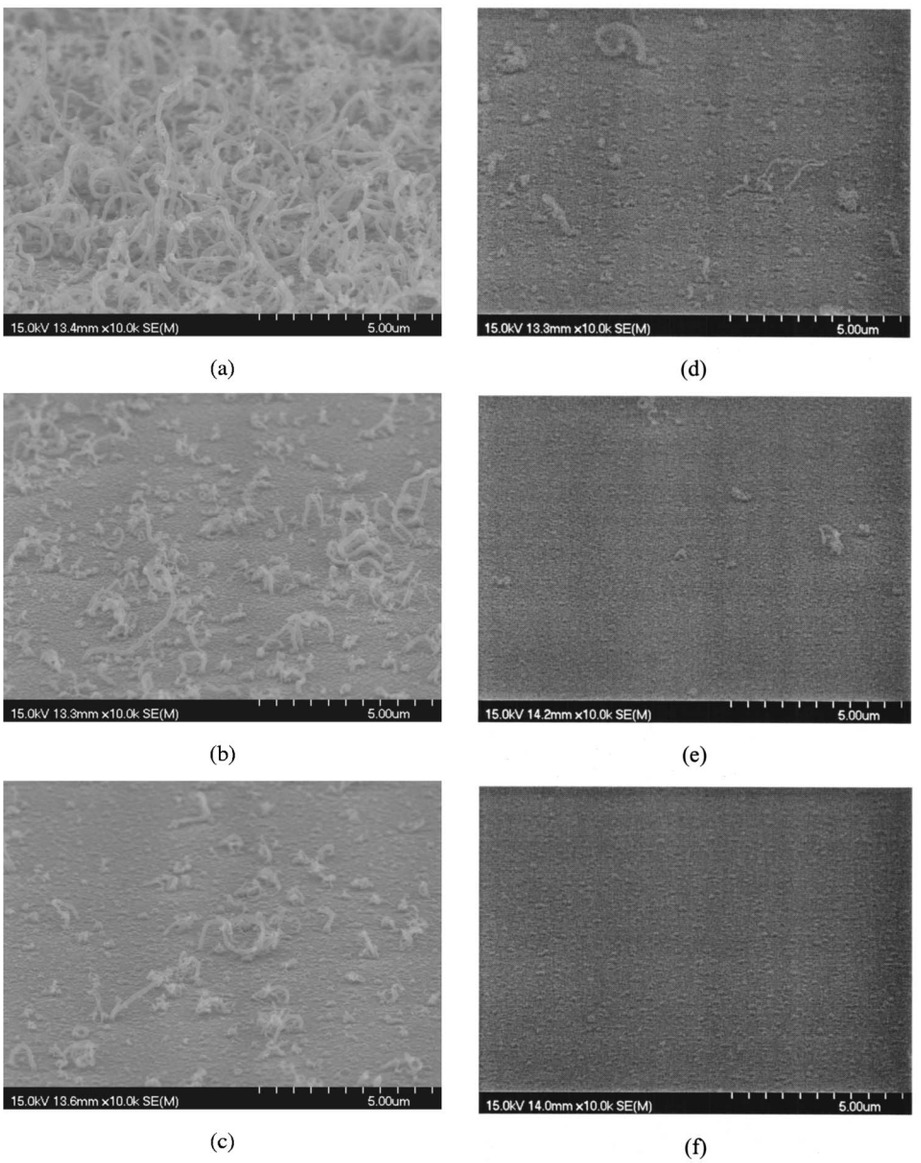

Figure 3. SEM images of carbon nanotubes with different thicknesses of the thin Ti capping layer: (a) 0, (b) 10, (c) 20, (d) 40, (e) 100, and (f) 200 Å.

of carbon nanotubes without the thin Ti capping layer reaches as high as 400 mA/cm^2 for the first 6 s and decreases abruptly to almost zero in a very short time. Because the initial emission current of carbon nanotubes without the thin Ti capping layer is too high, data in the first 6 s are removed from Fig. 10b to make these two curves in the same scale. As shown in Fig. 10b, the emission current density of carbon nanotubes with the thin Ti capping layer keeps about 7 mA/cm^2 for 5 min then drop to 3 mA/cm^2 and decrease very slowly in the next 55 min. From the SEM image of the sample without a thin Ti capping layer after measurement (Fig. 11), it can be observed that all carbon nanotubes disappear and only some amorphous-carbon-like material are left after the measurement at 10 V/μm for 1 h. This destructive phenomenon may result from the Joule heating, which was probably generated from the high contact resistance between the carbon nanotubes and the substrate with a high current density passing through. The sample with the thin Ti capping layer can reduce the contact resistance between carbon nanotubes and the substrate hence suppress the Joule heating. The improvement of the adhesion and the contact resistance between the carbon nanotubes and the substrate may result from the combination of the thin Ti capping layer and the Ti buffer layer during the growth of carbon nanotubes at 700°C.

Conclusions

Via depositing a thin Ti capping layer on the hydrogen-pretreated catalytic nanopaticles, the density of carbon nanotubes can be efficiently modified to promote the electric characteristics of field emission. From the experimental results, there is an appropriate thickness, 20 Å, of the thin Ti capping layer which can optimizes the emission current density of carbon nanotubes. With 20 Å thin Ti capping layer, the turn-on field of 2.5 V/μm and threshold field of 3.5 V/μm are obtained at the turn-on current of 10 μA/cm^2 and the threshold current of 10 mA/cm^2. In this case, the density of carbon nanotubes is about 2×10^7 cm^{-2} which roughly matches the simulation results for suppressing the screening effect. Furthermore, the thin Ti capping layer is also favorable to the reliability issues. The breakdown field has been increased and the phenomenon of Joule

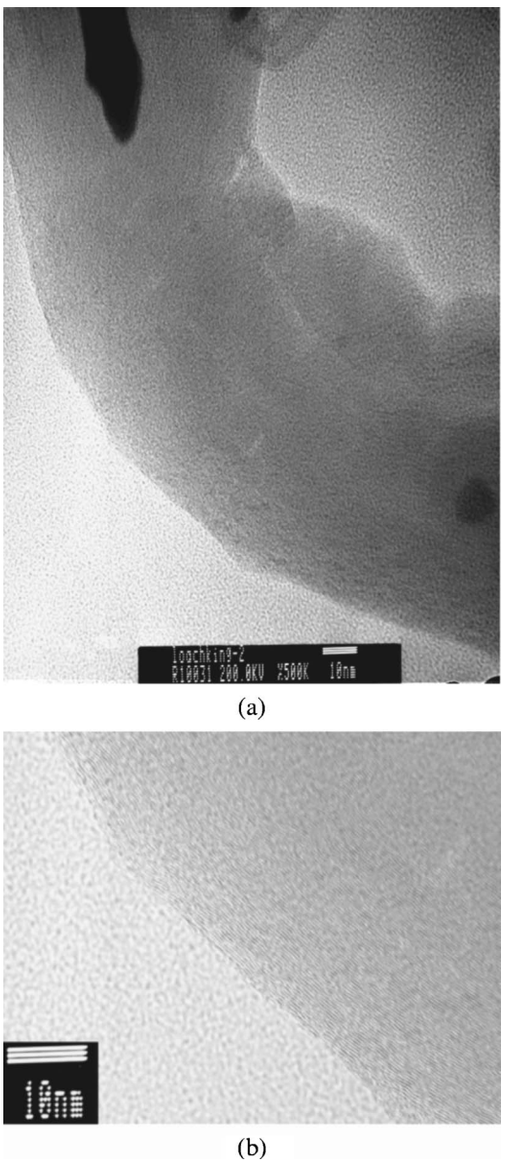

Figure 4. TEM images of (a) carbon nanotube with a nanoparticle contained and (b) carbon nanotube in higher resolution.

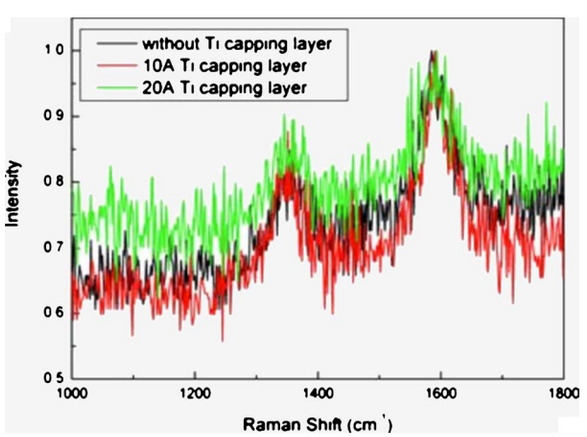

Figure 5. (Color online) The analysis of Raman spectra for CNTs in samples with 0, 10, and 20 Å Ti capping layers.

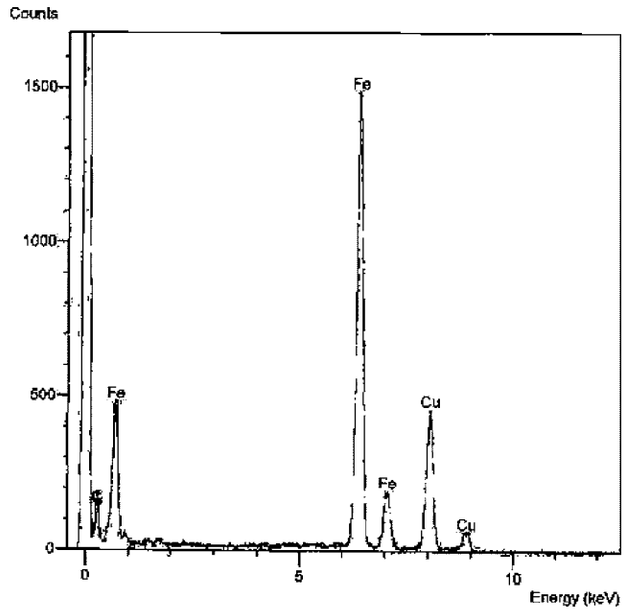

Figure 6. EDS analysis of the nanoparticle in the carbon nanotube.

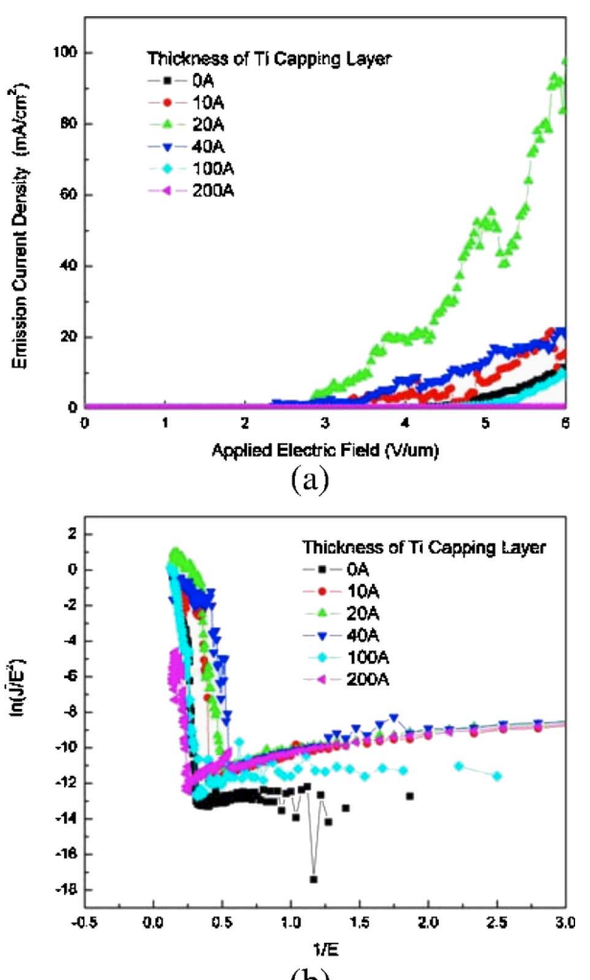

Figure 7. (Color online) The characteristics of field emission. (a) The emission current density vs applied electric field and (b) the Fowler-Nordheim plot.

Table I. The turn-on field and threshold field of the carbon nanotubes with different thicknesses of the thin Ti capping layers.

	Thickness of thin Ti capping layer (Å)					
	0 Å	10 Å	20 Å	40 Å	100 Å	200 Å
$E_{\text{turn-on}}$ (V/μm)	3.8	2.6	2.5	2.1	3.9	4.7
E_{th} (V/μm)	5.9	5.2	3.5	4.6	6	N. A.

Table II. The density of the carbon nanotubes with different thicknesses of the thin Ti capping layers.

	Thickness of thin Ti capping layer (Å)					
	0 Å	10 Å	20 Å	40 Å	100 Å	200 Å
Density of CNTs (point/cm^2)	$10^8 \sim 10^9$	10^8	2×10^7	7×10^6	4×10^6	0

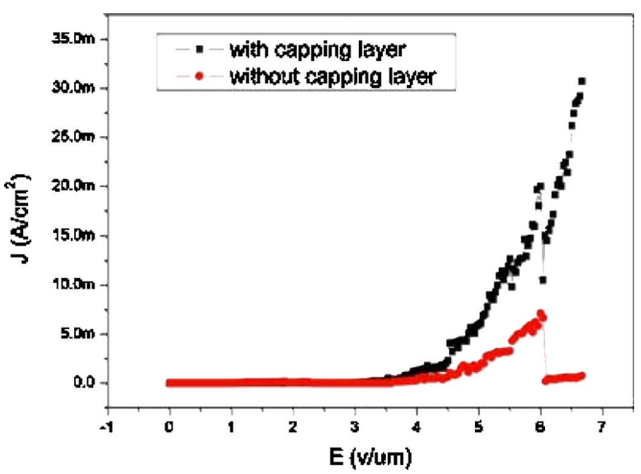

Figure 8. (Color online) J-E curve of carbon nanotubes with and without the thin Ti capping layer.

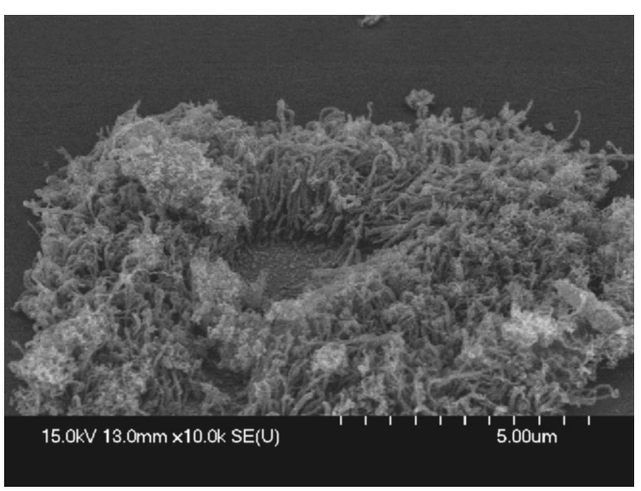

Figure 9. SEM image of carbon nanotubes with the thin Ti capping layer after electrical breakdown.

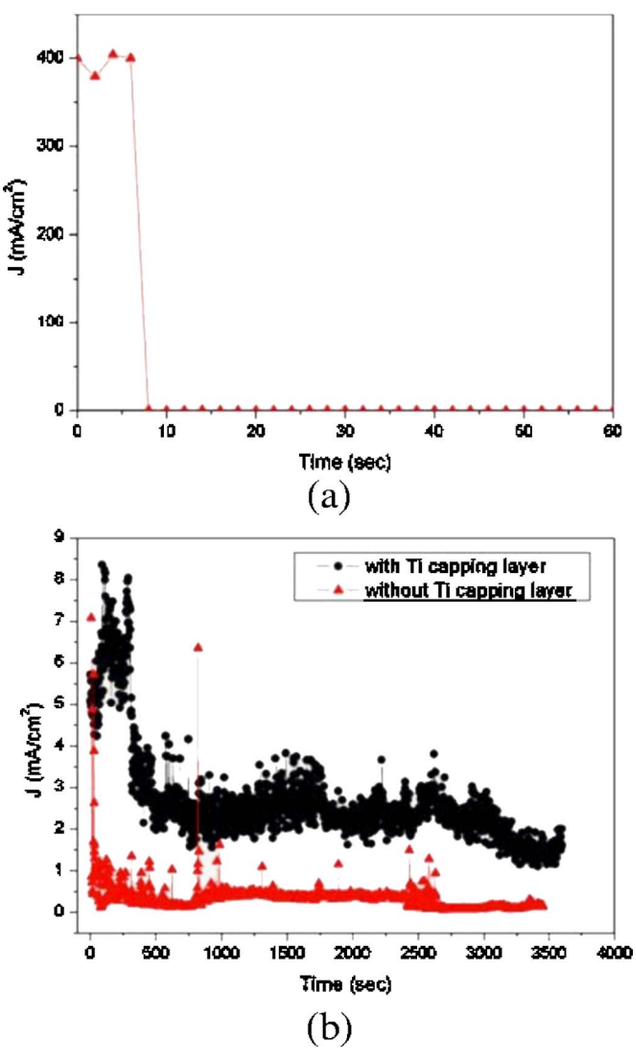

Figure 10. (Color online) (a) The emission current density vs time of carbon nanotubes without the thin Ti capping layer for the first minute and (b) the emission current density vs time of carbon nanotubes with and without the thin Ti capping layer for 1 h.

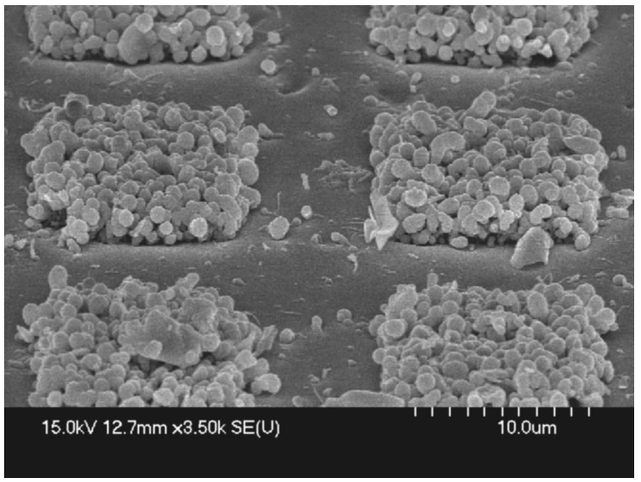

Figure 11. SEM image of carbon nanotubes without thin Ti capping layer after measurement at 10 V/μm for 1 h.

heating has also been significantly suppressed by means of the thin Ti capping layer after pretreatment. Two main reasons are conjectured to improve the reliability. One is the better adhesion between carbon nanotubes and the substrate which may suppress the mechanical destruction and prevent the emitters from the electrical breakdown. The other is the lower contact resistance between the carbon nanotubes and the substrate, which may reduce the Joule heating when the devices are operated with high current density. Therefore, a thin Ti capping layer on hydrogen-pretreated catalytic iron nanoparticles is a very promising method to suppress the screening effect and improve the reliability of carbon nanotubes.

Acknowledgments

This research was supported in part by the National Science Council of Taiwan under contract no. SC94-2218-E-009-028. Technical support from the Nano Facility Center (Semiconductor Research Center) of National Chiao Tung University is also acknowledged.

National Chiao-Tung University assisted in meeting the publication costs of this article.

References

1. S. Iijima, *Nature (London)*, **354**, 56 (1991).
2. Y. Saito, M. Okuda, N. Fujimoto, T. Yoshikawa, M. Tomita, and T. Hayashi, *Jpn. J. Appl. Phys., Part 1*, **33**, L526 (1994).
3. Y. J. Park, I. T. Han, H. J. Kim, N. S. Lee, Y. W. Jin, J. W. Kim, J. E. Jung, C. Y. Park, and J. MinKim, *Jpn. J. Appl. Phys., Part 1*, **42**, 1414 (2003).
4. Y.-S. Woo, I. T. Han, Y. J. Park, H. J. Kim, J. E. Jung, N. S. Lee, D. Y. Jeon, and J. M. Kim, *Jpn. J. Appl. Phys., Part 1*, **42**, 1410 (2003).
5. C. Mi, C.-M. Ch. Shi, and C.-F. Chen, *Jpn. J. Appl. Phys., Part 1*, **42**, 614 (2003).
6. Y. Huh, J. Y. Lee, and C. J. Lee, *Jpn. J. Appl. Phys., Part 1*, **42**, 7154 (2003).
7. T. Ikuno, M. Katayama, N. Yamauchi, W. Wongwiriyapan, S.-I. Honda, K. Oura, R. Hobara, and S. Hasegawa, *Jpn. J. Appl. Phys., Part 1*, **43**, 860 (2004).
8. R. Martel, T. Schimdt, H. R. Shea, and P. Avouris, *Appl. Phys. Lett.*, **73**, 2447 (1998).
9. W. A. de Heer, A. Chateline, and D. Ugrate, *Science*, **270**, 1179 (1995).
10. H. Dai, J. H. Hafner, A. G. Rinzler, D. T. Colbert, and R. E. Smalley, *Nature (London)*, **388**, 756 (1997).
11. H. Dai, N. Franklin, and J. Han, *Appl. Phys. Lett.*, **73**, 1508 (1998).
12. K. Shibayama, M. Hiraki, Y. Saito, and A. Hosong, *Jpn. J. Appl. Phys., Part 1*, **42**, 3698 (2003).
13. J. M. Kim, W. B. Choi, N. S. Lee, and J. E. Jung, *Diamond Relat. Mater.*, **9**, 1184 (2000).
14. R. H. Fowler and L. Nordheim, *Proc. R. Soc. London, Ser. A*, **119**, 173 (1928).
15. T. E. Stern, B. S. Grossling, and R. H. Fowler, *Proc. R. Soc. London, Ser. A*, **124**, 699 (1929).
16. D. Temple, *Mater. Sci. Eng., R.*, **24**, 185 (1999).
17. O. Gröning, O. M. Küttel, Ch. Emmenegger, P. Gröning, and L. Schlapbach, *J. Vac. Sci. Technol. B*, **18**, 665 (2000).
18. C.-P. Juan, K.-J. Chen, C.-C. Tsai, K.-C. Lin, W.-K. Hong, C.-Y. Hsieh, W.-P. Wang, R.-L. Lai, K.-H. Chen, L.-C. Chen, and H.-C. Cheng, *Jpn. J. Appl. Phys., Part 1*, **44**, 365 (2005).
19. C.-P. Juan, C.-C. Tsai, K.-H. Chen, L.-C. Chen, and H.-C. Cheng, *Jpn. J. Appl. Phys., Part 1*, **44**, 8231 (2005).
20. L. Dong, A. Subramanian, B. J. Nelson, and Y. Sun, in *Intelligent Robots and Systems 2005*, p. 3598 (2005).
21. Y. C. Choi, Y. M. Shin, S. C. Lim, D. J. Bae, Y. H. Lee, and B. S. Lee, *J. Appl. Phys.*, **88**, 4898 (2000).
22. M. Okai, T. Fujieda, K. Hidaka, T. Muneyoshi, and T. Yaguchi, *Jpn. J. Appl. Phys., Part 1*, **44**, 2051 (2005).
23. K. A. Dean, T. P. Burgin, and B. R. Chalamala, *Appl. Phys. Lett.*, **79**, 1873 (2001).
24. J.-M. Bonard and C. Klinke, *Phys. Rev. B*, **67**, 115406 (2003).
25. C. Liu, A.-j. Cheng, M. Clark, and Y. Tzeng, *Diamond Relat. Mater.*, **14**, 835 (2005).
26. M. Wang, K. P. Pramoda, and S. H. Goh, *Carbon*, **44**, 613 (2006).
27. J.-H. Han, S. H. Lee, A. S. Berdinskiy, Y. W. Kim, J.-B. Yoo, C.-Y. Park, J. J. Choi, T. Jung, I. T. Han, and J. M. Kim, *Diamond Relat. Mater.*, **14**, 1891 (2005).
28. J. H. Park, J. S. Moon, J. H. Han, A. S. Berdinskiy, D. G. Kuvshinov, J. B. Yoo, C. Y. Park, J. W. Nam, J. H. Park, C. G. Lee, and D. H. Choe, *Diamond Relat. Mater.*, **14**, 1463 (2005).